THE JOURNAL OF PHYSICAL CHEMISTRY C

Article

pubs.acs.org/JPCC

Temperature- and Pressure-Dependent Hydrogen Concentration in Supported PdH_x Nanoparticles by Pd K-Edge X-ray Absorption Spectroscopy

Aram L. Bugaev,*[,†] Alexander A. Guda,[†] Kirill A. Lomachenko,[†,‡] Vasiliy V. Srabionyan,[†] Lusegen A. Bugaev,*[,†] Alexander V. Soldatov,[†] Carlo Lamberti,[†,‡] Vladimir P. Dmitriev,[§] and Jeroen A. van Bokhoven[∥,⊥]

[†]Southern Federal University, Zorge Street 5, 344090 Rostov-on-Don, Russia

[‡]Department of Chemistry, NIS and CrisDI Centers, Turin University and INSTM Reference Center, Via P. Giuria 7, 10125 Turin, Italy

[§]Polygone Scientifique Louis Néel, SNBL at ESRF, 6 rue Jules Horowitz, 38000 Grenoble, France

[∥]Institute for Chemical and Bioengineering, ETH Zurich, HCI E127 8093 Zurich, Switzerland

[⊥]Laboratory for Catalysis and Sustainable Chemistry (LSK) Swiss Light Source, Paul Scherrer Institute, Villigen, Switzerland

Supporting Information

ABSTRACT: Hydride formation in palladium nanoparticles was studied by Pd K-edge X-ray absorption spectroscopy in both the near-edge (XANES) and the extended (EXAFS) regions and by X-ray diffraction (XRD) both *in situ* as a function of temperature and hydrogen pressure. In contrast to EXAFS and XRD, which probe Pd–Pd interatomic distance changes, the direct effect of hydrogen concentration on the electronic palladium structure is observed in the intensities and the peak positions in the XANES region. By using theoretical simulations, we propose a simple analysis of hydrogen concentration based on the changes of relative peak amplitudes in the XANES region, which correlate with interatomic distance changes determined by both EXAFS and XRD. By the quantitative analysis of XANES difference spectra, we have developed a scheme to determine the hydrogen concentration in palladium nanoparticles without applying any additional calibration procedures with alternative experimental techniques.

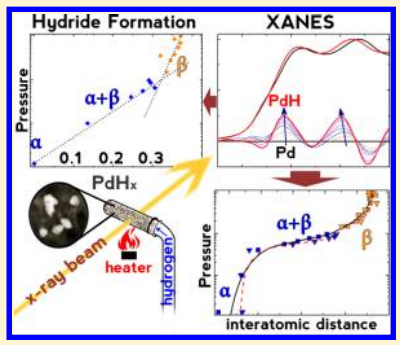

1. INTRODUCTION

Metal nanoparticles (NPs) have been the subject of extensive experimental[1−6] and theoretical[7−9] investigations. Metal NPs find applications in several fields, such as catalysis,[3,6,10−14] electrochemistry,[15] imaging,[16,17] sensing,[18] biology,[16−19] and medicine.[20,21] Synchrotron radiation in general and X-ray absorption spectroscopy in particular have played a determinant role in understanding the structure and the reactivity of metal NPs.[3,4,6,14,22−27]

Palladium nanoparticles[28] are extensively studied in order to achieve the best performance of important catalytic reactions: hydrogenation of petroleum resin,[29] abatement of hydrocarbons,[30−32] CO and NO_x emissions, hydrogenation of unsaturated hydrocarbons, purification of terephthalic acid,[33,34] and synthesis of fine chemicals (e.g., active pharmaceutical ingredients).[35−37] Palladium absorbs hydrogen, and palladium hydride formation strongly affects the catalytic performance of the catalyst.[38−41] In particular, bulk-dissolved or subsurface hydrogen, which is more energetic than surface hydrogen, can hydrogenate surface adsorbates upon emerging to the surface.[42,43] The (P,T) phase diagram and hydrogen desorption kinetics are strongly affected by the size of the nanoclusters.[42,44−46] In small palladium nanoclusters the hydride phase is destabilized,[47] but the phase separation is still observed down to 1.5 nm size.[42,48−50] Theoretical simulations indicate that concentration of hydrogen is higher in the subsurface layers while the core region of palladium nanoparticle is hydrogen-depleted.[51−53]

Formation of palladium hydride is accompanied by lattice expansion and thus can be detected by X-ray diffraction (XRD).[54,55] Changes of dielectric properties of the medium during hydrogenation shift the wavelength and the width plasmonic resonance curves. Indirect nanoplasmonic sensing calibrated with quartz crystal microbalance measurements was applied for *in situ* investigation of isotherms for hydrogen absorption and kinetics of hydrogen release from small nanoparticles.[45] An increase of interatomic Pd–Pd distances in palladium hydride nanoparticles was also efficiently detected by extended X-ray absorption fine structure (EXAFS) at the Pd K-edge.[56−59] Unlike other experimental techniques, the Pd L_3 edge X-ray absorption near edge structure (XANES) enables the direct observation of the formation of palladium

Received: January 21, 2014
Revised: March 20, 2014
Published: April 23, 2014

dx.doi.org/10.1021/jp500734p | J. Phys. Chem. C 2014, 118, 10416−10423

hydrides[50,60−64] since new antibonding states form in palladium hydride which can be detected due to the sensitivity of the L_3-XANES to the unoccupied density of d-electronic states (d-DOS). Palladium hydride thus gives rise to a signature peak at ~6 eV above the Fermi level.[63]

It is worth noticing that in the presence of weak backscattering hydrogen atoms the PdH_x phase can be directly probed by X-ray absorption techniques. This is far to be a trivial point, as very few examples can be found in the literature where H atoms should be taken into account in theoretical models to improve the agreement with the experimental results. This is the case e.g. of the light $NaAlH_4$ alloy for hydrogen storage[65] and of cations[66−73] and anions[74] in water solution.

In this paper we use XANES, EXAFS, and XRD measurements and theoretical simulations of XANES to quantitatively determine the evolution of the palladium local atomic and electronic structures in palladium nanoclusters supported by Al_2O_3. Furthermore, we demonstrate how the hydrogen concentration can be directly determined by the fitting of the XANES spectra.

2. EXPERIMENTAL METHODS

X-ray absorption and diffraction measurements were carried out at the Swiss-Norwegian Beamline (BM01B) of the European Synchrotron Radiation Facility (ESRF), Grenoble, France. We used a glass capillary 1.0 mm in diameter which was filled with about 50 mm Pd/Al_2O_3 powder, fixed from both sides by quartz wool (see Figure S1). The capillary was installed in a metal sample holder and was connected to a remotely controlled gas rig enabling to control the hydrogen pressure using accurate pneumatic valves. A scroll pump was connected to the system to be able to evacuate the sample, and the minimal pressure obtained in the experiment was about 1 mbar. The capillary was open from the both sides, which enabled us to tune hydrogen pressure without affecting the position of the sample inside the capillary as the pressure gradient was acting equally from both sides. Temperature was controlled by means of a gas blower, positioned under the sample. According to the specific calibration datasheet of the heater, the range of the constant temperature flow was larger than the horizontal beam size. The size of X-ray beam was 1.0 mm × 0.3 mm. In each of the selected points of the pressure−temperature space, both X-ray absorption and diffraction measurements were performed. Pd K-edge EXAFS data were collected in transmission mode using ionization chambers in the energy range of 24.1−25.4 keV employing a Si(111) monochromator in the continuous scanning mode. Pd foil was measured simultaneously with the sample as a reference compound to monitor possible energy drift.[75]

Before each absorption measurement, five diffraction patterns were recorded by the CMOS-Dexela 2D detector. Both the wavelength $\lambda = 0.513\,23$ Å and the sample-to-detector distance $D_{SD} = 343.25$ mm were calibrated using a silicon powder model sample. This setup allowed collecting diffraction patterns with 2θ values between 5° and 40°. Subsequent averaging and integration were carried out using Fit2D software[76] while WinPLOTR code included in the FullProf Suite[77] was employed for the peak fitting.

EXAFS data were processed by the IFEFFIT package,[78] including background removal, normalization, energy shift correction, Fourier transformation, and fitting using theoretical amplitude and phase functions calculated by the FEFF6 code.[79] Single-shell real-space fit between 1.5 and 3.0 Å was performed to k^2-weighted normalized data in the k-range of 5−12 Å^{-1}. The fit was performed with the following variable parameters: the Pd−Pd interatomic distance (R_{Pd-Pd}), the Debye−Waller factor (σ^2), energy shift (ΔE_0), and coordination number (N). The parameters ΔE_0 and N were considered as common variables for all spectra. To reduce the number of variable parameters, the fit of the spectra measured during isobaric heating was performed applying the temperature dependence $\sigma^2(T)$ of the Debye correlation model.[80] The value of the reduction factor $S_0^2 = 0.82$ was used the same as in Pd foil.

Theoretical simulations of the K-edge XANES spectra were performed using the full multiple scattering approach with the Hedin−Lundqvist exchange correlation potential[81] implemented in the FEFF8.4 code[79,82] The simulations were tested for the atomic clusters with radii from 3 to 10 Å, and convergence was reached already at 7.5 Å. Quantitative analysis of the experimental Pd K-edge XANES spectra was performed using the multidimensional interpolation approach[83] realized in FitIt 3.01 code.[84]

3. RESULTS AND DISCUSSION

3.1. Sample Characterization. Palladium nanoparticles on Al_2O_3 support were prepared by the incipient wetness impregnation method as described elsewhere.[50,85,86] Preliminary characterization was performed by means of transmission electron microscopy (TEM) in Z-contrast mode using a JEM-2010F FasTEMm FEI electron microscope (manufactured by JEOL) operated at 200 kV with an extracting voltage of 4500 V.

TEM measurements shown in Figure 1 identified the average size of palladium nanoparticles $\bar{D}$ = 9.5 nm counting 100

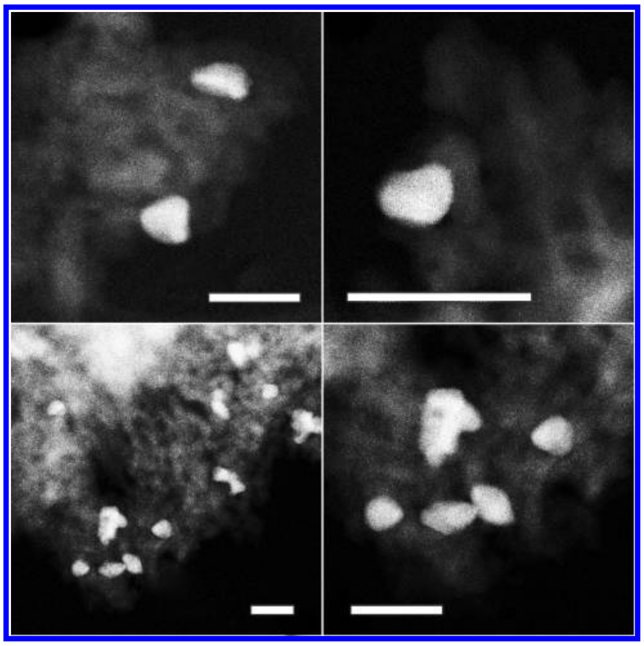

Figure 1. TEM images of the palladium nanoparticles deposited on Al_2O_3. Scale bars are 20 nm.

particles (see Figure S2 in Supporting Information). No difference in size distribution before the experiment and after hydrogen absorption and desorption was observed.

The crystalline size distribution was also obtained by analyzing fwhm of Pd (111) reflection using a L&TGSD program[87] which realizes the FW$^1/_5/^4/_5$M method by measuring the width at $^1/_5$ and $^4/_5$ height of the peak (for

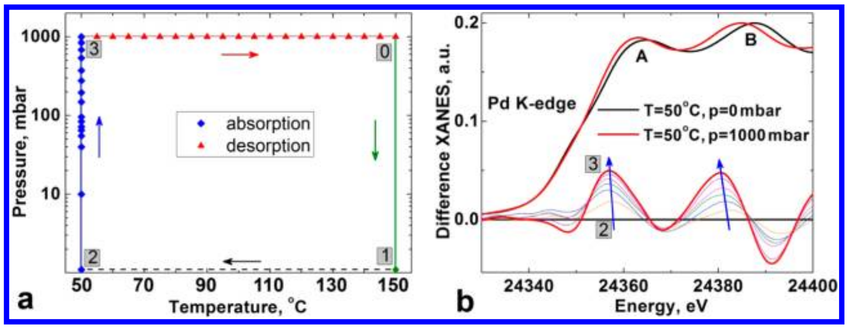

Figure 2. (a) Experimental (P,T) conditions. Scattered points correspond to the (P,T) conditions at which both EXAFS and XRD data were collected. Blue diamonds and red triangles correspond to isothermal hydrogen absorption and isobaric hydrogen desorption, respectively. (b) Difference Pd K-edge XANES spectra of the palladium nanoparticles at 50 °C and at different hydrogen pressure from point 2 to point 3 obtained after subtracting the spectrum of bare palladium nanoparticles (taken at point 50 °C). Arrows indicate increasing hydrogen pressure. For better visualization, conventional XANES spectra were multiplied by 0.2.

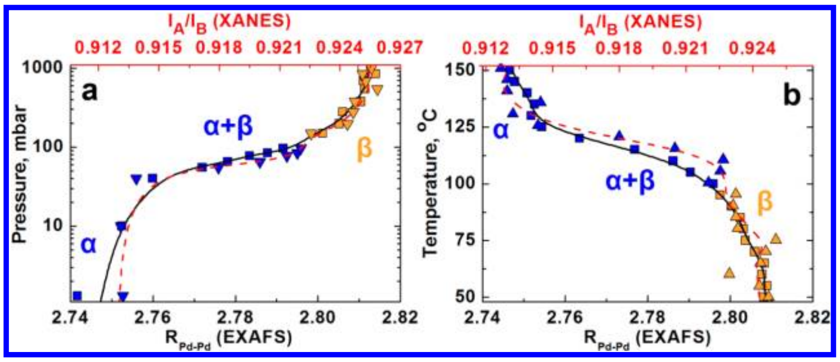

Figure 3. Correlation between the Pd−Pd interatomic distance obtained from EXAFS (squares, black solid line) and the ratio I_A/I_B of XANES first peaks intensities (triangles, red dashed line). Blue and orange colors correspond to $\alpha + \beta$ and β phases of the palladium hydride, respectively.

details, see Supporting Information). We obtained the average nanocrystalline size of 5.2 nm (see Figure S3). It is less than suggested by microscopy, since the coherent scattering regions could be smaller than the average grain size visualized by TEM due to the partial agglomeration of the nanoparticles.

3.2. Experimental Pd K-Edge EXAFS and XANES. Figure 2a illustrates the changes of hydrogen pressure and temperature during the experiment. To remove surface oxygen, palladium nanoparticles were exposed to 1 bar of pure hydrogen for 30 min at 150 °C (point 0), then evacuated (point 1), and cooled down to 50 °C in a vacuum (point 2). Two series of EXAFS spectra were collected: (1) during isothermal hydrogen absorption (points 2−3) at 50 °C and stepwise increasing hydrogen pressure from 10^{-3} to 1 bar and (2) during isobaric hydrogen desorption (points 3−0) at 1 bar of H_2 and stepwise increasing temperature from 50 to 150 °C with steps ΔT = 5 °C.

The EXAFS analysis (vide infra) showed that during the isothermal absorption of hydrogen the Pd−Pd interatomic distances increased from 2.74 ± 0.01 to 2.81 ± 0.01 Å. Despite the fact that the absolute error in determining interatomic distances by EXAFS is about 0.01 Å,[14,88] the relative changes ΔR can be determined with much better accuracy,[89,90] typically better than 0.005 Å, so more than 15 different distances can be trustfully resolved in the 2.74−2.81 Å interval. After the isobaric desorption the Pd−Pd interatomic distances decreased to 2.75 ± 0.01 Å. The expansion data of Pd lattice during hydrogen uptake were also observed in XRD by fitting the Pd (111) peak. The interatomic distances increase from 2.74 to 2.79 Å, which is less than the increase of the distances obtained from EXAFS (Figure S6). This difference is remarkable, and it may stem from an effect of lower hydrogen concentration in the core of a nanoparticle than in the surface region.[51−53] However, at high hydrogen concentrations Pd (111) reflection overlaps with the one of Al_2O_3 substrate, which could have affected the fitting results (see Supporting Information).

Lattice expansion associated with the palladium hydride phase in supported palladium nanoparticles was observed even at low (10 mbar) hydrogen pressures. During the isothermal hydrogen absorption at 50 °C the most intense lattice expansion was registered for the hydrogen pressure between 40 and 100 mbar. The interatomic distances obtained for the spectra taken at T = 50 °C and P = 1000 mbar correspond to the expansion of palladium lattice by 2.5%. The most intense lattice contraction during the isobaric hydrogen desorption at 1000 mbar H_2 occurred after heating above 100 °C. The Pd−Pd interatomic distance at 150 °C and 1000 mbar hydrogen is the same as in initial bare palladium nanoparticles (within the accuracy of the method), so the observed hydride formation was reversible.

The coordination number decreased from 12 in Pd foil to 9.8 in the nanoparticles. The Debye−Waller factor increased by 0.001 $Å^2$ for the hydride phase, which suggests an inhomogeneous hydrogen distribution inside the palladium nanoparticle. This redistribution may be either disordered, caused by a statistical population of octahedral interstices by hydrogen atoms, or core−shell-like, similarly to the one observed in theoretical calculations for the metal.[51−53] In the case of the core−shell-like structure, the Debye−Waller factor can be decreased by the refinements of the fitting procedure as was demonstrated for bare palladium nanoparticles.[91] Because of the changes in d-density of electron states under hydride

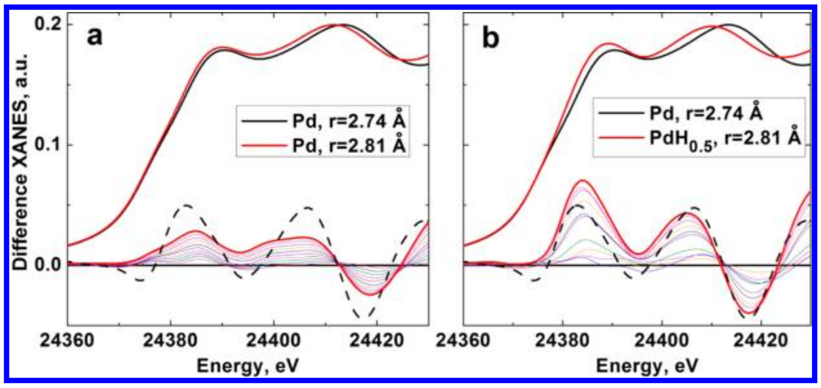

Figure 4. Difference theoretical Pd K-edge XANES spectra (a) for palladium cluster with variable interatomic distances without hydrogen atoms and (b) with hydrogen concentration taken into consideration. Dashed line corresponds to experimental difference spectrum of palladium hydride at 1000 mbar. The final spectrum (bold red) corresponds to $PdH_{0.5}$ with Pd−Pd interatomic distance r = 2.81 Å. For better visualization, conventional XANES spectra were multiplied by the factor of 0.2.

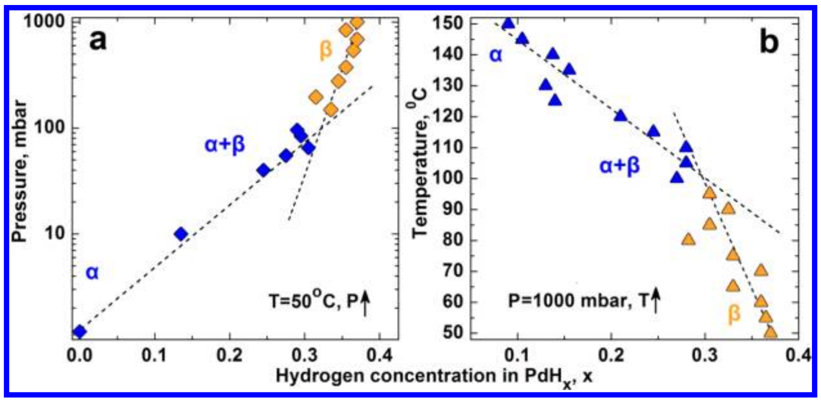

Figure 5. Hydrogen concentration as a function of (a) pressure and (b) temperature determined by quantitative XANES fitting. Dashed lines are for demonstrative purposes only. Blue and orange colors correspond to $\alpha + \beta$ and β phases of the palladium hydride, respectively.

formation, Pd L_3-edge XANES spectra were usually considered as a main source of information on hydrogen concentration. However, acquisition of soft X-ray Pd L_3-edge spectra is experimentally more demanding in the *in situ* conditions under H_2 pressure. Therefore, we use Pd K-edge XANES which reflects the changes in the unoccupied electronic p-states during hydride formation.[92]

Figure 2b shows the changes of near-edge region of absorption spectra. The peak B at 24 388 eV for the bare palladium shifts to the lower energies with the increase of hydrogen pressure. The peak A at 24 364 eV also shifts to the lower energies, and its intensity increases relatively to the intensity of the peak B. Theoretical calculations of the palladium electronic structure indicated that the increase of peak A intensity is associated with the mixing of Pd d-states with hydrogen s- and p-unoccupied states (see Figure S8). As we show below, the relation of intensities of these peaks can be used for qualitative analysis of the palladium hydride formation.

According to the standard PdH phase diagrams for the bulk systems[93] and that obtained for the palladium nanoparticles by indirect nanoplasmonic sensing[45] and thermogravimetric analysis,[94] our results shown in Figure 3 indicate the pure β phase formation. It is also evident that the intensity ratio I_A/I_B of the first near-edge peaks correlates with the interatomic distance obtained from EXAFS. This tendency was also predicted by theoretical simulations.[92] The simple utilization of experimental XANES by measuring only first peaks intensities makes this technique very useful for *in situ* measurements of relative changes of hydrogen concentration in palladium hydride under varying external conditions. Nevertheless, such analysis gives only relative changes of H concentration in palladium nanoparticle. In the next section we show that the absolute values can be determined by simultaneous theoretical fitting of EXAFS and XANES spectra with variable hydrogen concentration.

3.3. XANES Simulations and Fitting Procedure. Theoretical simulations (Figure 4) illustrate the role of hydrogen in the spectral shape of Pd K-edge XANES. Utilizing difference spectra, we have demonstrated that the spectra, calculated using a simple model of palladium clusters with formal increase of only lattice parameter, are not in agreement with the experimental data, which is evident from the difference spectra (Figure 4a).

To simulate the hydrogenated samples, hydrogen atoms were included in the cluster model. Different hydrogen concentrations, from bare Pd to $PdH_{0.5}$, were simulated by placing H atoms in octahedral interstitials of the Pd lattice with the given probability using a Monte Carlo approach.[95] To obtain proper statistical distribution, 1000 different hydride structures were randomly generated for each concentration. XANES spectra were then calculated for each structure and consequently averaged. The calculated spectra for such model reproduce all experimental features including the monotonic increase of the ratio I_A/I_B and the shift of the first near-edge peaks to the lower energies.

To obtain the concentration of hydrogen at each experimental point in Figure 2a, difference XANES spectra were further analyzed by the multidimensional interpolation approach[83] of FitIt 3.01 code.[84] Theoretical spectra for bare Pd, $PdH_{0.3}$, and $PdH_{0.5}$ with Pd−Pd interatomic distances of 2.75, 2.78, and 2.81 Å, respectively, were taken as interpolation nodes. The interpolation polynomial was constructed as $r + x + r^2 + x^2 + r{\cdot}x$, where the parameters r and x correspond to interatomic distance and hydrogen concentration, respectively. The fit was performed for both conventional XANES and difference spectra, yielding similar results.

Figure 5 illustrates the hydrogen concentration obtained by quantitative fitting XANES data taken at different H pressures during isothermal hydrogen absorption. We have determined that the highest hydrogen concentration x in PdH_x obtained for the spectrum taken at 50 °C and 1000 mbar of hydrogen was equal to 0.36 ± 0.03. The data points were highlighted by two dashed lines with different slope. The intersection point of these lines at $x \approx 0.3$ corresponds to the transition to β-phase of palladium hydride. The obtained concentrations and the point of phase transition are consistent with the results obtained by indirect nanoplasmonic sensing[45] and thermogravimetric analysis.[94]

4. CONCLUSIONS

The hydride phase formation in the palladium nanoparticles was studied *in situ* by near-edge and extended X-ray absorption spectroscopies above Pd K-edge. Although EXAFS analysis reveals the changes in Pd−Pd interatomic distances under hydride phase formation, it does not allow determining the absolute values of hydrogen concentration in PdH_x nanoparticles. Therefore, we have suggested a new approach to evaluate the absolute values of hydrogen concentration in palladium nanoparticles during hydrogen absorption/desorption process using X-ray absorption data. By theoretical analysis of Pd K-edge XANES spectra, we have shown that the presence of hydrogen atoms in Pd lattice has a direct effect on the shape and the intensities of first near-edge peaks of the spectrum, so that the ratio of these intensities can be used for the fast and simple qualitative estimation of hydrogen concentration in Pd nanoparticles. Absolute values of hydrogen concentration in the palladium nanoparticles during hydrogen absorption/desorption were obtained by fitting experimental XANES with theoretical spectra for models generated using the Monte Carlo approach. The obtained results indicate a nonlinear dependence of the Pd−Pd interatomic distances upon the hydrogen concentration during the β-phase formation.

■ ASSOCIATED CONTENT

Supporting Information

Description of grain size distribution (GZD) algorithm, XRD fitting procedure, size distribution obtained from TEM and XRD, EXAFS data, XARD data, interatomic distances by EXAFS vs XRD, interatomic distance dependence upon H concentration, calculated density of electronic states. This material is available free of charge via the Internet at http://pubs.acs.org.

■ AUTHOR INFORMATION

Corresponding Authors

*Phone +7 863 219 8775; e-mail abugaev@sfedu.ru (A.L.B.).
*Phone +7 863 297 5336; e-mail bugaev@sfedu.ru (L.A.B.).

Notes

The authors declare no competing financial interest.

■ ACKNOWLEDGMENTS

A.V.S. and C.L. acknowledge the Mega-grant of the Russian Federation Government to support scientific research under the supervision of the leading scientist at Southern Federal University, No. 14.Y26.31.0001, for the partial funding of the research. A.L.B., A.A.G., and K.A.L. acknowledge the Grant of the President of Russia for Young Scientists MK-3206.2014.2. Authors are grateful to the SNBL staff for allocation of the beam time and technical support during the experiments.

■ REFERENCES

(1) Astruc, D.; Lu, F.; Aranzaes, J. R. Nanoparticles as recyclable catalysts: The frontier between homogeneous and heterogeneous catalysis. *Angew. Chem., Int. Ed.* **2005**, *44*, 7852−7872.

(2) Watanabe, K.; Menzel, D.; Nilius, N.; Freund, H. J. Photochemistry on metal nanoparticles. *Chem. Rev.* **2006**, *106*, 4301−4320.

(3) Singh, J.; Lamberti, C.; van Bokhoven, J. A. Advanced X-ray absorption and emission spectroscopy: in situ catalytic studies. *Chem. Soc. Rev.* **2010**, *39*, 4754−4766.

(4) Frenkel, A. I. Applications of extended X-ray absorption fine-structure spectroscopy to studies of bimetallic nanoparticle catalysts. *Chem. Soc. Rev.* **2012**, *41*, 8163−8178.

(5) Bordiga, S.; Groppo, E.; Agostini, G.; van Bokhoven, J. A.; Lamberti, C. Reactivity of surface species in heterogeneous catalysts probed by in situ X-ray absorption techniques. *Chem. Rev.* **2013**, *113*, 1736−1850.

(6) Mino, L.; Agostini, G.; Borfecchia, E.; Gianolio, D.; Piovano, A.; Gallo, E.; Lamberti, C. Low-dimensional systems investigated by x-ray absorption spectroscopy: a selection of 2D, 1D and 0D cases. *J. Phys. D: Appl. Phys.* **2013**, *46*, 423001.

(7) Bonacickoutecky, V.; Fantucci, P.; Koutecky, J. Quantum-chemistry of small clusters of elements of group-Ia, group-Ib, and group-Iia - Fundamental-concepts, predictions, and interpretation of experiments. *Chem. Rev.* **1991**, *91*, 1035−1108.

(8) (a) Baletto, F.; Ferrando, R. Structural properties of nanoclusters: Energetic, thermodynamic, and kinetic effects. *Rev. Mod. Phys.* **2005**, *77*, 371−423. (b) Morton, S. M.; Silverstein, D. W.; Jensen, L. Theoretical studies of plasmonics using electronic structure methods. *Chem. Rev.* **2011**, *111*, 3962−3994.

(9) Agostini, G.; Bertinetti, L.; Piovano, A.; Pellegrini, R.; Leofanti, G.; Groppo, E.; Lamberti, C. The effect of different fcc nanoparticle distributions on particle size and surface area determination: a theoretical study. *J. Phys. Chem. C* **2014**, *118*, 4085−4094.

(10) Crooks, R. M.; Zhao, M. Q.; Sun, L.; Chechik, V.; Yeung, L. K. Dendrimer-encapsulated metal nanoparticles: Synthesis, characterization, and applications to catalysis. *Acc. Chem. Res.* **2001**, *34*, 181−190.

(11) Moreno-Manas, M.; Pleixats, R. Formation of carbon-carbon bonds under catalysis by transition-metal nanoparticles. *Acc. Chem. Res.* **2003**, *36*, 638−643.

(12) Eustis, S.; El-Sayed, M. A. Why gold nanoparticles are more precious than pretty gold: Noble metal surface plasmon resonance and its enhancement of the radiative and nonradiative properties of nanocrystals of different shapes. *Chem. Soc. Rev.* **2006**, *35*, 209−217.

(13) Shylesh, S.; Schunemann, V.; Thiel, W. R. Magnetically separable nanocatalysts: Bridges between homogeneous and heterogeneous catalysis. *Angew. Chem., Int. Ed.* **2010**, *49*, 3428−3459.

(14) Bordiga, S.; Groppo, E.; Agostini, G.; van Bokhoven, J. A.; Lamberti, C. Reactivity of surface species in heterogeneous catalysts probed by in situ X-ray absorption techniques. *Chem. Rev.* **2013**, *113*, 1736−1850.

(15) Murray, R. W. Nanoelectrochemistry: Metal nanoparticles, nanoelectrodes, and nanopores. *Chem. Rev.* **2008**, *108*, 2688−2720.

(16) Jain, P. K.; Huang, X. H.; El-Sayed, I. H.; El-Sayed, M. A. Noble metals on the nanoscale: optical and photothermal properties and some applications in imaging, sensing, biology, and medicine. *Acc. Chem. Res.* **2008**, *41*, 1578−1586.

(17) Murphy, C. J.; Gole, A. M.; Stone, J. W.; Sisco, P. N.; Alkilany, A. M.; Goldsmith, E. C.; Baxter, S. C. Gold nanoparticles in biology: beyond toxicity to cellular imaging. *Acc. Chem. Res.* **2008**, *41*, 1721−1730.

(18) Anker, J. N.; Hall, W. P.; Lyandres, O.; Shah, N. C.; Zhao, J.; Van Duyne, R. P. Biosensing with plasmonic nanosensors. *Nat. Mater.* **2008**, *7*, 442−453.

(19) Hu, M.; Chen, J. Y.; Li, Z. Y.; Au, L.; Hartland, G. V.; Li, X. D.; Marquez, M.; Xia, Y. N. Gold nanostructures: engineering their plasmonic properties for biomedical applications. *Chem. Soc. Rev.* **2006**, *35*, 1084−1094.

(20) El-Sayed, I. H.; Huang, X. H.; El-Sayed, M. A. Surface plasmon resonance scattering and absorption of anti-EGFR antibody conjugated gold nanoparticles in cancer diagnostics: Applications in oral cancer. *Nano Lett.* **2005**, *5*, 829−834.

(21) Lal, S.; Clare, S. E.; Halas, N. J. Nanoshell-enabled photothermal cancer therapy: impending clinical impact. *Acc. Chem. Res.* **2008**, *41*, 1842−1851.

(22) Frenkel, A. I.; Hills, C. W.; Nuzzo, R. G. A view from the inside: Complexity in the atomic scale ordering of supported metal nanoparticles. *J. Phys. Chem. B* **2001**, *105*, 12689−12703.

(23) Knecht, M. R.; Weir, M. G.; Frenkel, A. I.; Crooks, R. M. Structural rearrangement of bimetallic alloy PdAu nanoparticles within dendrimer templates to yield core/shell configurations. *Chem. Mater.* **2008**, *20*, 1019−1028.

(24) Cuenya, B. R.; Croy, J. R.; Mostafa, S.; Behafarid, F.; Li, L.; Zhang, Z. F.; Yang, J. C.; Wang, Q.; Frenkel, A. I. Solving the structure of size-selected Pt nanocatalysts synthesized by inverse micelle encapsulation. *J. Am. Chem. Soc.* **2010**, *132*, 8747−8756.

(25) Frenkel, A. I.; Yevick, A.; Cooper, C.; Vasic, R. Modeling the structure and composition of nanoparticles by extended X-ray absorption fine-structure spectroscopy. *Annu. Rev. Anal. Chem.* **2011**, *4*, 23−39.

(26) Li, Y. M.; Liu, J. H. C.; Witham, C. A.; Huang, W. Y.; Marcus, M. A.; Fakra, S. C.; Alayoglu, P.; Zhu, Z. W.; Thompson, C. M.; Arjun, A.; Lee, K.; Gross, E.; Toste, F. D.; Somorjai, G. A. A Pt-cluster-based heterogeneous catalyst for homogeneous catalytic reactions: X-ray absorption spectroscopy and reaction kinetic studies of their activity and stability against leaching. *J. Am. Chem. Soc.* **2011**, *133*, 13527−13533.

(27) Anderson, R. M.; Zhang, L.; Loussaert, J. A.; Frenkel, A. I.; Henkelman, G.; Crooks, R. M. An experimental and theoretical investigation of the inversion of Pd@Pt core@shell dendrimer-encapsulated nanoparticles. *ACS Nano* **2013**, *7*, 9345−9353.

(28) Tungler, A.; Tarnai, T.; Hegedus, L.; Fodor, K.; Máthé, T. Palladium-mediated heterogeneous catalytic hydrogenations: selectivity of liquid-phase reactions for the fine chemicals industry. *Platinum Met. Rev.* **1998**, *42*, 108−115.

(29) Yu, L. J.; Jiang, D. H.; Xu, J.; Ma, L.; Li, X. N. Two-stage hydrogenation modification of C-9 petroleum resin over NiWS/gamma-Al_2O_3 and PdRu/gamma-Al_2O_3 catalysts in series. *China Pet. Process. Petrochem. Technol.* **2012**, *14*, 83−89.

(30) Gelin, P.; Primet, M. Complete oxidation of methane at low temperature over noble metal based catalysts: a review. *Appl. Catal., B* **2002**, *39*, 1−37.

(31) Lampert, J. K.; Kazi, M. S.; Farrauto, R. J. Palladium catalyst performance for methane emissions abatement from lean burn natural gas vehicles. *Appl. Catal., B* **1997**, *14*, 211−223.

(32) Liotta, L. F. Catalytic oxidation of volatile organic compounds on supported noble metals. *Appl. Catal., B* **2010**, *100*, 403−412.

(33) Pellegrini, R.; Agostini, G.; Groppo, E.; Piovano, A.; Leofanti, G.; Lamberti, C. 0.5 wt.% Pd/C catalyst for purification of terephthalic acid: Irreversible deactivation in industrial plants. *J. Catal.* **2011**, *280*, 150−160.

(34) Pernicone, N.; Cerboni, M.; Prelazzi, G.; Pinna, F.; Fagherazzi, G. An investigation on Pd/C industrial catalysts for the purification of terephthalic acid. *Catal. Today* **1998**, *44*, 129−135.

(35) Blaser, H. U.; Indolese, A.; Schnyder, A.; Steiner, H.; Studer, M. Supported palladium catalysts for fine chemicals synthesis. *J. Mol. Catal. A: Chem.* **2001**, *173*, 3−18.

(36) Garrett, C. E.; Prasad, K. The art of meeting palladium specifications in active pharmaceutical ingredients produced by Pd-catalyzed reactions. *Adv. Synth. Catal.* **2004**, *346*, 889−900.

(37) Torborg, C.; Beller, M. Recent applications of palladium-catalyzed coupling reactions in the pharmaceutical, agrochemical, and fine chemical industries. *Adv. Synth. Catal.* **2009**, *351*, 3027−3043.

(38) Chase, Z. A.; Fulton, J. L.; Camaioni, D. M.; Mei, D.; Balasubramanian, M.; Pham, V.-T.; Zhao, C.; Weber, R. S.; Wang, Y.; Lercher, J. A. State of supported pd during catalysis in water. *J. Phys. Chem. C* **2013**, *117*, 17603−17612.

(39) Haug, K.; Buergi, T.; Trautman, T.; Ceyer, S. Distinctive reactivities of surface-bound H and bulk H for the catalytic hydrogenation of acetylene. *J. Am. Chem. Soc.* **1998**, *120*, 8885−8886.

(40) Johnson, A.; Daley, S.; Utz, A.; Ceyer, S. The chemistry of bulk hydrogen: reaction of hydrogen embedded in nickel with adsorbed CH_3. *Science* **1992**, *257*, 223−225.

(41) Teschner, D.; Borsodi, J.; Wootsch, A.; Revay, Z.; Havecker, M.; Knop-Gericke, A.; Jackson, S. D.; Schlögl, R. The roles of subsurface carbon and hydrogen in palladium-catalyzed alkyne hydrogenation. *Science* **2008**, *320*, 86−89.

(42) Ingham, B.; Toney, M. F.; Hendy, S. C.; Cox, T.; Fong, D. D.; Eastman, J. A.; Fuoss, P. H.; Stevens, K. J.; Lassesson, A.; Brown, S. Particle size effect of hydrogen-induced lattice expansion of palladium nanoclusters. *Phys. Rev. B* **2008**, *78*, 245408−245412.

(43) Morkel, M.; Rupprechter, G.; Freund, H.-J. Finite size effects on supported Pd nanoparticles: Interaction of hydrogen with CO and C_2H_4. *Surf. sci.* **2005**, *588*, L209−L219.

(44) (a) Agostini, G.; Lamberti, C.; Pellegrini, R.; Leofanti, G.; Giannici, F.; Longo, A.; Groppo, E. Effect of pre-reduction on the properties and the catalytic activity of Pd/carbon catalysts: A comparison with Pd/Al_2O_3. *ACS Catal.* **2014**, *4*, 187−194. (b) Groppo, E.; Agostini, G.; Piovano, A.; Muddada, N. B.; Leofanti, G.; Pellegrini, R.; Portale, G.; Longo, A.; Lamberti, C. Effect of reduction in liquid phase on the properties and the catalytic activity of Pd/Al_2O_3 catalysts. *J. Catal.* **2012**, *287*, 44−54. (c) Groppo, E.; Agostini, G.; Borfecchia, E.; Wei, L.; Giannici, F.; Portale, G.; Longo, A.; Lamberti, C. Formation and growth of Pd nanoparticles inside a highly cross-linked polystyrene support: role of the reducing agent. *J. Phys. Chem. C* **2014**, *118*, 8406−8415.

(45) Langhammer, C.; Larsson, E. M.; Kasemo, B.; Zoric, I. Indirect nanoplasmonic sensing: ultrasensitive experimental platform for nanomaterials science and optical nanocalorimetry. *Nano Lett.* **2010**, *10*, 3529−3538.

(46) Yamauchi, M.; Ikeda, R.; Kitagawa, H.; Takata, M. Nanosize effects on hydrogen storage in palladium. *J. Phys. Chem. C* **2008**, *112*, 3294−3299.

(47) Bérubé, V.; Radtke, G.; Dresselhaus, M.; Chen, G. Size effects on the hydrogen storage properties of nanostructured metal hydrides: a review. *Int. J. Energy Res.* **2007**, *31*, 637−663.

(48) Jobic, H.; Renouprez, A. Formation of hydrides in small particles of palladium supported in Y-zeolite. *J. Less-Common Met.* **1987**, *129*, 311−316.

(49) Narehood, D.; Kishore, S.; Goto, H.; Adair, J.; Nelson, J.; Gutierrez, H.; Eklund, P. X-ray diffraction and H-storage in ultra-small palladium particles. *Int. J. Hydrogen Energy* **2009**, *34*, 952−960.

(50) Tew, M. W.; Miller, J. T.; van Bokhoven, J. A. Particle size effect of hydride formation and surface hydrogen adsorption of nanosized palladium catalysts: L-3 edge vs K edge X-ray absorption spectroscopy. *J. Phys. Chem. C* **2009**, *113*, 15140−15147.

(51) Langhammer, C.; Zhdanov, V. P.; Zorić, I.; Kasemo, B. Size-dependent hysteresis in the formation and decomposition of hydride in metal nanoparticles. *Chem. Phys. Lett.* **2010**, *488*, 62−66.

(52) Langhammer, C.; Zhdanov, V. P.; Zorić, I.; Kasemo, B. Size-dependent kinetics of hydriding and dehydriding of Pd nanoparticles. *Phys. Rev. Lett.* **2010**, *104*, 135502−135504.
(53) Zhdanov, V. P.; Kasemo, B. Kinetics of the formation of a new phase in nanoparticles. *Chem. Phys. Lett.* **2008**, *460*, 158−161.
(54) Suleiman, M.; Jisrawi, N.; Dankert, O.; Reetz, M.; Bähtz, C.; Kirchheim, R.; Pundt, A. Phase transition and lattice expansion during hydrogen loading of nanometer sized palladium clusters. *J. Alloys Compd.* **2003**, *356*, 644−648.
(55) Vogel, W.; He, W.; Huang, Q.-H.; Zou, Z.; Zhang, X.-G.; Yang, H. Palladium nanoparticles "breathe" hydrogen; a surgical view with X-ray diffraction. *Int. J. Hydrogen Energy* **2010**, *35*, 8609−8620.
(56) Agostini, G.; Pellegrini, R.; Leofanti, G.; Bertinetti, L.; Bertarione, S.; Groppo, E.; Zecchina, A.; Lamberti, C. Determination of the particle size, available surface area, and nature of exposed sites for silica− alumina-supported Pd nanoparticles: A multitechnical approach. *J. Phys. Chem. C* **2009**, *113*, 10485−10492.
(57) Davis, R.; Landry, S.; Horsley, J.; Boudart, M. X-ray-absorption study of the interaction of hydrogen with clusters of supported palladium. *Phys. Rev. B* **1989**, *39*, 10580−10583.
(58) McCaulley, J. A. In-situ X-ray absorption spectroscopy studies of hydride and carbide formation in supported palladium catalysts. *J. Phys. Chem.* **1993**, *97*, 10372−10379.
(59) Scarano, D.; Bordiga, S.; Lamberti, C.; Ricchiardi, G.; Bertarione, S.; Spoto, G. Hydrogen adsorption and spill-over effects on H−Y and Pd-containing Y zeolites. *Appl. Catal., A* **2006**, *307*, 3−12.
(60) Bianconi, A.; Soldatov, A. V.; Ivanchenko, T. I. Confirmation of hydrogen-induced unoccupied states in PdH: multiple-scattering analysis of palladium L1 and L3 XANES. *Nucl. Instrum. Methods, A* **1991**, *308*, 248−250.
(61) Davoli, I.; Marcelli, A.; Fortunato, G.; D'Amico, A.; Coluzza, C.; Bianconi, A. Palladium L_3 absorption edge of $PdH_{0.6}$ films: Evidence for hydrogen induced unoccupied states. *Solid State Commun.* **1989**, *71*, 383−390.
(62) Ruckman, M.; Reisfeld, G.; Jisrawi, N.; Weinert, M.; Strongin, M.; Wiesmann, H.; Croft, M.; Sahiner, A.; Sills, D.; Ansari, P. XANES study of hydrogen incorporation in a Pd-capped Nb thin film. *Phys. Rev. B* **1998**, *57*, 3881−3886.
(63) Soldatov, A.; Della Longa, S.; Bianconi, A. Relevant role of hydrogen atoms in the XANES of Pd hydride: Evidence of hydrogen induced unoccupied states. *Solid State Commun.* **1993**, *85*, 863−868.
(64) Witjens, L. C.; Bitter, J. H.; van Dillen, A. J.; de Jong, K. P.; de Groot, F. M. F. Pd L_3 edge XANES investigation of the electronic and geometric structure of Pd/Ag-H membranes. *Phys. Chem. Chem. Phys.* **2004**, *6*, 3903−3906.
(65) Balde, C. P.; Mijovilovich, A. E.; Koningsberger, D. C.; van der Eerden, A. M. J.; Smith, A. D.; de Jong, K. P.; Bitter, J. H. XAFS study of the AlK-edge in $NaAlH_4$. *J. Phys. Chem. C* **2007**, *111*, 11721−11725.
(66) D'Angelo, P.; Pavel, N. V. EXAFS and molecular dynamics studies of ionic solutions. *J. Synchrotron Radiat.* **2001**, *8*, 173−177.
(67) D'Angelo, P.; Benfatto, M.; Della Longa, S.; Pavel, N. V. Combined XANES and EXAFS analysis of Co^{2+}, Ni^{2+}, and Zn^{2+} aqueous solutions. *Phys. Rev. B* **2002**, *66*, No. 064209.
(68) D'Angelo, P.; Barone, V.; Chillemi, G.; Sanna, N.; Meyer-Klaucke, W.; Pavel, N. V. Hydrogen and higher shell contributions in Zn^{2+}, Ni^{2+}, and Co^{2+} aqueous solutions: An X-ray absorption fine structure and molecular dynamics study. *J. Am. Chem. Soc.* **2002**, *124*, 1958−1967.
(69) Chillemi, G.; D'Angelo, P.; Pavel, N. V.; Sanna, N.; Barone, V. Development and validation of an integrated computational approach for the study of ionic species in solution by means of effective two-body potentials. The case of Zn^{2+}, Ni^{2+}, and Co^{2+} in aqueous solutions. *J. Am. Chem. Soc.* **2002**, *124*, 1968−1976.
(70) D'Angelo, P.; Petit, P. E.; Pavel, N. V. Double-electron excitation channels at the Ca^{2+} K-edge of hydrated calcium ion. *J. Phys. Chem. B* **2004**, *108*, 11857−11865.
(71) D'Angelo, P.; Benfatto, M. Effect of multielectronic configurations on the XAFS analysis at the FeK edge. *J. Phys. Chem. A* **2004**, *108*, 4505−4514.
(72) Migliorati, V.; Mancini, G.; Chillemi, G.; Zitolo, A.; D'Angelo, P. Effect of the Zn^{2+} and Hg^{2+} ions on the structure of liquid water. *J. Phys. Chem. A* **2011**, *115*, 4798−4803.
(73) Migliorati, V.; Mancini, G.; Tatoli, S.; Zitolo, A.; Filipponi, A.; De Panfilis, S.; Di Cicco, A.; D'Angelo, P. Hydration properties of the Zn^{2+} ion in water at high pressure. *Inorg. Chem.* **2013**, *52*, 1141−1150.
(74) D'Angelo, P.; Migliorati, V.; Guidoni, L. Hydration properties of the bromide aqua ion: the interplay of first principle and classical molecular dynamics, and X-ray absorption spectroscopy. *Inorg. Chem.* **2010**, *49*, 4224−4231.
(75) Lamberti, C.; Bordiga, S.; Bonino, F.; Prestipino, C.; Berlier, G.; Capello, L.; D'Acapito, F.; Xamena, F. X. L. I.; Zecchina, A. Determination of the oxidation and coordination state of copper on different Cu-based catalysts by XANES spectroscopy in situ or in operando conditions. *Phys. Chem. Chem. Phys.* **2003**, *5*, 4502−4509.
(76) Hammersley, A. P.; Svensson, S. O.; Hanfland, M.; Fitch, A. N.; Hausermann, D. Two-dimensional detector software: From real detector to idealised image or two-theta scan. *High Pressure Res.* **1996**, *14*, 235−248.
(77) Roisnel, T.; Rodriquez-Carvajal, J. WinPLOTR: A Windows tool for powder diffraction pattern analysis. *Mater. Sci. Forum* **2001**, *378*, 118−123.
(78) Ravel, B.; Newville, M. ATHENA, ARTEMIS, HEPHAESTUS: data analysis for X-ray absorption spectroscopy using IFEFFIT. *J. Synchrotron Radiat.* **2005**, *12*, 537−541.
(79) Rehr, J. J.; Albers, R. C. Theoretical approaches to x-ray absorption fine structure. *Rev. Mod. Phys.* **2000**, *72*, 621−654.
(80) Beni, G.; Platzman, P. Temperature and polarization dependence of extended X-ray absorption fine-structure spectra. *Phys. Rev. B* **1976**, *14*, 1514−1518.
(81) Hedin, L.; Lundqvist, B. I. Explicit local exchange-correlation potentials. *J. Phys. C* **1971**, *4*, 2064−2083.
(82) Rehr, J. J.; Ankudinov, A. L. Progress in the theory and interpretation of XANES. *Coord. Chem. Rev.* **2005**, *249*, 131−140.
(83) Smolentsev, G.; Soldatov, A. Quantitative local structure refinement from XANES: multi-dimensional interpolation approach. *J. Synchrotron Radiat.* **2005**, *13*, 19−29.
(84) Smolentsev, G.; Soldatov, A. V. FitIt: New software to extract structural information on the basis of XANES fitting. *Comput. Mater. Sci.* **2007**, *39*, 569−574.
(85) Tew, M. W.; Janousch, M.; Huthwelker, T.; van Bokhoven, J. A. The roles of carbide and hydride in oxide-supported palladium nanoparticles for alkyne hydrogenation. *J. Catal.* **2011**, *283*, 45−54.
(86) Tew, M. W.; Nachtegaal, M.; Janousch, M.; Huthwelker, T.; van Bokhoven, J. A. The irreversible formation of palladium carbide during hydrogenation of 1-pentyne over silica-supported palladium nanoparticles: in situ Pd K and L3 edge XAS. *Phys. Chem. Chem. Phys.* **2012**, *14*, 5761−5768.
(87) Leontyev, I.; Guterman, V.; Pakhomova, E.; Timoshenko, P.; Guterman, A.; Zakharchenko, I.; Petin, G.; Dkhil, B. XRD and electrochemical investigation of particle size effects in platinum-cobalt cathode electrocatalysts for oxygen reduction. *J. Alloys Compd.* **2010**, *500*, 241−246.
(88) Koningsberger, D.; Prins, R. *X-ray Absorption: Principles, Applications, Techniques of EXAFS, SEXAFS and XANES*; John Wiley & Sons: New York, 1987.
(89) Pettifer, R. F.; Mathon, O.; Pascarelli, S.; Cooke, M. D.; Gibbs, M. R. Measurement of femtometre-scale atomic displacements by X-ray absorption spectroscopy. *Nature* **2005**, *435*, 78−81.
(90) Romanato, F.; De Salvador, D.; Berti, M.; Drigo, A.; Natali, M.; Tormen, M.; Rossetto, G.; Pascarelli, S.; Boscherini, F.; Lamberti, C.; Mobilio, S. Bond-length variation in $In_xGa_{1-x}As$/InP strained epitaxial layers. *Phys. Rev. B* **1998**, *57*, 14619−14622.
(91) Srabionyan, V. V.; Bugaev, A. L.; Pryadchenko, V. V.; Avakyan, L. A.; van Bokhoven, J. A.; Bugaev, L. A. EXAFS study of size

dependence of atomic structure in palladium nanoparticles. *J. Phys. Chem. Solids* **2014**, *75*, 470−476.

(92) Bugaev, A. L.; Srabionyan, V. V.; Soldatov, A. V.; Bugaev, L. A.; van Bokhoven, J. A. The role of hydrogen in formation of Pd XANES in Pd-nanoparticles. *J. Phys. Conf. Ser.* **2013**, *430*, 012028−012033.

(93) Manchester, F. D.; San-Martin, A.; Pitre, J. M. The H-Pd (hydrogen-palladium) system. *J. Phase Equilib.* **1994**, *15*, 62−83.

(94) Kishore, S.; Nelson, J.; Adair, J.; Eklund, P. Hydrogen storage in spherical and platelet palladium nanoparticles. *J. Alloys Compd.* **2005**, *389*, 234−242.

(95) Hammersley, J. M.; Handscomb, D. C.; Weiss, G. Monte Carlo methods. *Phys. Today* **1965**, *18*, 55.